

MICROCOPY RESOLUTION TEST CHART  
25 - 1000

AFWAL-TR-85-4154

RESEARCH ON MECHANICAL PROPERTIES  
FOR ENGINE LIFE PREDICTION



N. E. ASHBAUGH  
M. KHOBAIB  
G. A. HARTMAN  
T. WEERASOORIYA  
A. M. RAJENDRAN  
D. C. MAXWELL  
R. C. GOODMAN

UNIVERSITY OF DAYTON  
RESEARCH INSTITUTE  
DAYTON, OHIO 45469

MAY 1986

INTERIM REPORT FOR PERIOD  
1 AUGUST 1984 THROUGH 31 JULY 1985

APPROVED FOR PUBLIC RELEASE; DISTRIBUTION IS UNLIMITED.

THIS FILE COPY

MATERIALS LABORATORY  
AIR FORCE WRIGHT AERONAUTICAL LABORATORIES  
AIR FORCE SYSTEMS COMMAND  
WRIGHT-PATTERSON AIR FORCE BASE, OHIO 45433-6533

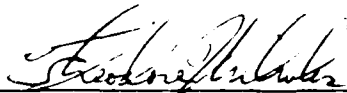
AD-A169 570

NOTICE

When Government drawings, specifications, or other data are used for any purpose other than in connection with a definitely related Government procurement operation, the United States Government thereby incurs no responsibility nor any obligation whatsoever; and the fact that the government may have formulated, furnished, or in any way supplied the said drawings, specifications, or other data, is not to be regarded by implication or otherwise as in any manner licensing the holder or any other person or corporation, or conveying any rights or permission to manufacture use, or sell any patented invention that may in any way be related thereto.

This report has been reviewed by the Office of Public Affairs (ASD/PA) and is releasable to the National Technical Information Service (NTIS). At NTIS, it will be available to the general public, including foreign nations.

This technical report has been reviewed and is approved for publication.

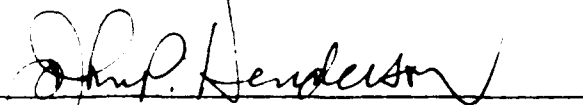


THEODORE NICHOLAS  
Project Engineer  
Metals Behavior Branch



ALLAN W. GUNDERSON  
Technical Area Manager  
Metals Behavior Branch

FOR THE COMMANDER



JOHN P. HENDERSON, Chief  
Metals Behavior Branch  
Metals & Ceramics Division

If your address has changed, if you wish to be removed from our mailing list, or if the addressee is no longer employed by your organization please notify AFWAL/MLLN, W-PAFB, OH 45433 to help us maintain a current mailing list.

Copies of this report should not be returned unless return is required by security considerations, contractual obligations, or notice on a specific document.

Classified

CLASSIFICATION OF THIS PAGE

REPORT DOCUMENTATION PAGE

AD-A169570

1. SECURITY CLASSIFICATION Classified		1b. RESTRICTIVE MARKINGS	
2. SECURITY CLASSIFICATION AUTHORITY		3. DISTRIBUTION/AVAILABILITY OF REPORT Approved for public release; distribution is unlimited.	
4. SECURITY CLASSIFICATION DOWNGRADING SCHEDULE		5. MONITORING ORGANIZATION REPORT NUMBER(S) AFWAL-TR-85-4154	
6. PERFORMING ORGANIZATION REPORT NUMBER(S) R-85-132		7a. NAME OF MONITORING ORGANIZATION Materials Laboratory (AFWAL/MLLN) Air Force Wright Aeronautical Laboratories	
7b. ADDRESS (City, State and ZIP Code) College Park Drive Dayton, Ohio 45469		7c. ADDRESS (City, State and ZIP Code) Wright-Patterson AFB, Ohio 45433-6533	
8. FUNDING/SPONSORING ORGANIZATION AFWAL/MLLN		9. PROCUREMENT INSTRUMENT IDENTIFICATION NUMBER F33615-84-C-5051	
10. SOURCE OF FUNDING NOS.		11. TITLE	
PROGRAM ELEMENT NO. 61102F	PROJECT NO. 2307	TASK NO. P1	WORK UNIT NO. 18
12. AUTHOR(S) N. E. Ashbaugh, M. Khobaib, G. A. Hartman, S. S. Sooriya, A. M. Rajendran, D. C. Maxwell, and R. C. Goodman			
13. TIME COVERED FROM 8/1/84 to 7/31/85		14. DATE OF REPORT (Yr., Mo., Day) May 1986	
15. PAGE COUNT 63		16. SUBJECT TERMS (Continue on reverse if necessary and identify by block number) Fatigue crack growth, crack growth behavior, crack growth threshold, creep, hot corrosion creep rupture, modeling, nickel-base superalloys, single crystals, interferometry,	
17. ABSTRACT (Continue on reverse if necessary and identify by block number) Analytical and experimental investigations have been performed to determine crack growth behavior of metals under conditions typical of the service environment of aircraft turbine engines. To evaluate baseline crack growth behavior, investigations have been conducted at elevated temperature in vacuum. The work performed can be divided into three general categories -- development of experimental and automation techniques, material characterization testing, and analytic studies. An automated laser interferometric displacement-measurement system using linear gratings has been developed. Enhancements of existing systems for the measurement of crack lengths and displacements are described. A number of computer automation techniques are also described. Fatigue and creep crack growth tests and creep rupture and hot corrosion tests were performed. Descriptions of the experimental techniques and the results for these tests are given.			
18. AVAILABILITY OF ABSTRACT UNLIMITED <input type="checkbox"/> SAME AS RPT <input type="checkbox"/> DTIC USERS <input checked="" type="checkbox"/>		21. ABSTRACT SECURITY CLASSIFICATION Unclassified	
22a. TELEPHONE NUMBER (Include Area Code) 255-2689		22b. OFFICE SYMBOL AFWAL/MLLN	

FORM 1473, 83 APR

EDITION OF 1 JAN 73 IS OBSOLETE

Unclassified

SECURITY CLASSIFICATION OF THIS PAGE

BLOCK 18 (Concluded)

crack-length-determination techniques, material test automation.

BLOCK 19 (Concluded)

are included. Results of analytical investigations in both material modeling and methodology development are presented, including discussions of applications within the laboratory.

## FOREWORD

The work described in this report was performed at the Metals Behavior Branch, Metals and Ceramics Division, Materials Laboratory, Air Force Wright Aeronautical Laboratories (AFWAL/MLLN) under Contract No. F33615-84-C-5051, "Research on Mechanical Properties for Engine Life Prediction." The contract is administered under the direction of AFWAL by Dr. Theodore Nicholas (MLLN). The program is being conducted by the Structural Integrity Division, University of Dayton Research Institute, Dayton, Ohio with Dr. Noel E. Ashbaugh as the Principal Investigator. This report is the first annual report on the progress on the three year contract.

The investigations were conducted by Drs. Noel E. Ashbaugh, M. Khobaib, Tusit Weerasooriya, A. M. Rajendran, and Messers. George Hartman, III and Dave Koester. Generation of the data was accomplished in part by Messers. Richard Goodman, David Maxwell, George Ahrens, David Johnson, William Goddard, and Mrs. Susan Ramsey. Assistance in data reduction, computer programming, fabrication of fixtures, and assembling mechanical and electrical components has been provided by Messers. Paul Enderle and Joe Mueller and Miss Pat Bornhorst. Miss Debbie Garner was responsible for the typing of this document. This work was performed during the period 1 August 1984 to 31 July 1985.



Accession For	
NTIS GRA&I	
DTIC TAB	
Unannounced	
Justification	
By	
Distribution/	
Availability Codes	
Avail. and/or	
Dist	Special

## TABLE OF CONTENTS

<u>SECTION</u>		<u>PAGE</u>
1	INTRODUCTION	1
2	EXPERIMENTAL DEVELOPMENTS	2
	2.1 MEASUREMENT TECHNIQUES	2
	2.1.1 <u>Linear Array Laser Interferometer (LALI)</u>	2
	2.1.2 <u>Back-Face Strain Compliance for SE(T) Specimen</u>	2
	2.1.3 <u>DC Potential on MTS #8 - TMF Testing</u>	3
	2.1.4 <u>DC Potential for Creep Crack Length Determination</u>	3
	2.1.5 <u>Specimen Illumination for Crack Length Measurement at 2000°F+</u>	4
	2.1.6 <u>Elevated Temperature 2000°F+ Furnace</u>	5
	2.2 TEST SYSTEM AUTOMATION	5
	2.2.1 <u>Improvements in the C20 System</u>	6
	2.2.2 <u>Installation of VIC-20 on Instron M/M</u>	6
	2.2.3 <u>Development of IDG Short Crack Testing System</u>	6
	2.2.4 <u>IBM System 9000 Installation on MTS #4 Vacuum System</u>	11
	2.2.5 <u>Automated Closure Load Determination</u>	11
	2.2.6 <u>Software Enhancements</u>	12
3	MATERIAL CHARACTERIZATION TESTS	15
	3.1 FATIGUE CRACK GROWTH TESTING	15
	3.1.1 <u>TMF Baseline Testing</u>	15
	3.1.2 <u>HCF/LCF Initiation in IN718 - C10</u>	15

TABLE OF CONTENTS (Continued)

<u>SECTION</u>		<u>PAGE</u>
3.1.3	<u>HCF/LCF Initiation in N4+ - Instron M/M</u>	16
3.1.4	<u>HCF/LCF Initiation on Hastalloy X on C20</u>	17
3.1.5	<u>Fatigue Crack Growth in Alloy N4</u>	19
3.1.6	<u>Threshold Evaluation of IN718</u>	19
3.1.7	<u>Effect of Overloads on Alloy IN718</u>	20
3.1.8	<u>Surface Flaw/Short Crack in Ti Alloys</u>	21
3.1.9	<u>Modeling of IN718 Crack Growth Behavior</u>	21
3.2	CREEP CRACK GROWTH TESTS	24
3.2.1	<u>High Temperature Creep Crack Growth in Alloy N4 in Laboratory Air</u>	24
3.2.2	<u>High Temperature Creep Crack Growth in Alloy N4 in Vacuum</u>	24
3.2.3	<u>Fracture Surface Analysis of Creep Crack Growth Tested Specimens</u>	25
3.3	CREEP RUPTURE TESTS	25
3.3.1	<u>Creep Rupture Tests of Bare and Coated Alloy N4 in Air</u>	25
3.3.2	<u>Fracture Surface Evaluation of Creep Rupture Specimens</u>	28
3.4	HOT CORROSION TESTS	36
3.4.1	<u>Effect of Hot Corrosion on Creep Rupture Life of IN718</u>	36
3.4.2	<u>Hot Corrosion in Alloy Rene' 77 and Rene' 80</u>	36

TABLE OF CONTENTS (Concluded)

<u>SECTION</u>		<u>PAGE</u>
4	ANALYTICAL DEVELOPMENTS	37
4.1	BACK-FACE STRAIN ON SEN GEOMETRY	37
4.2	ANALYSIS OF DISK-SHAPED COMPACT SPECIMEN	37
4.3	THREE DIMENSIONAL ANALYSIS OF CURVED CRACK FRONT	39
4.4	VALIDATION OF BODNER-PARTOM ROUTINES IN SNAP	39
4.5	COMPLIANCE EXPRESSIONS FOR CT SPECIMENS	43
5	DATA MAINTENANCE AND TEST SUPPORT ACTIVITIES	45
5.1	DATA TRANSMISSION AND STORAGE	45
5.2	MLLS BRANCH TEST SUPPORT ACTIVITIES	45
5.3	ELECTRONICS FABRICATION AND REPAIR	46
	REFERENCES	47
	APPENDIX A - DESCRIPTION OF IDG SHORT CRACK TESTING SYSTEM	A-1

## LIST OF ILLUSTRATIONS

<u>FIGURE</u>		<u>PAGE</u>
1	Schematic Illustration of the Principle of Operation of the Interferometric Displacement Gage.	8
2	Schematic Illustration of the Computerized Interferometric System.	9
3	Typical Load Vs Crack-Mouth-Opening-Displacement Data and Differential Data are Shown for a Small Surface Crack Where $2C \approx 50 \mu\text{m}$ and $d_o \approx 50 \mu\text{m}$ .	10
4	Combined Cyclic and Hold-Time Loadings Applied by Automated Control Software.	13
5	(a) Modified TF-34 Spectrum, and (b) Simple Overload Spectrum.	14
6	HCF/LCF Specimen Configuration.	18
7	Crack Growth as a Function of Temperature, Frequency, and $K_{\text{max}}$ at $R=0.1$ for IN718.	23
8	Fracture Surface of Specimen Tested in Vacuum, Showing a Small Zone of Transdendritic Failure.	26
9	Fracture Surface of Specimen Tested in Air, Showing Zone of Interdendritic Failure.	27
10	Fracture Surface of a Creep Rupture Specimen Showing Crack Initiation from Surface.	29
11	Fracture Surface of a Creep Rupture Specimen Showing Shrinkage Pores.	30
12	Complex Faults and Dislocation Networks.	31
13	(a) Complex Faults at $1800^{\circ}\text{F}$ and (b) Complex Faults at $1600^{\circ}\text{F}$ .	32
14	Faults and Super-Dislocations.	33
15	Microtwins at $1600^{\circ}\text{F}$ .	34

LIST OF ILLUSTRATIONS (Concluded)

<u>FIGURE</u>		<u>PAGE</u>
16	Absence of Faults and Evidence of $a/2$ [110] Dislocation.	35
17	Mesh for Finite Element Analysis of DC(T), $a/W = 0.5$ , Specimen.	38
18	Finite Element Model of a Tensile Strip Specimen.	40
19	Loading Cycle.	41
20	Comparison Between the SNAP and the Direct Solutions for the Cyclic Loading Response.	44
A1	Block Diagram of the Hardware Setup for the MTS/IDG Short Crack System.	A-3

LIST OF TABLES

<u>TABLE</u>		<u>PAGE</u>
1	PARAMETERS FOR THE BODNER-PARTOM CONSTITUTIVE EQUATIONS (REFERENCE 12)	42

SECTION 1  
INTRODUCTION

This program emphasizes the experimental determination of the advanced mechanical properties, primarily the characterization of crack growth behavior of typical turbine engine disk and blade alloys under a broad range of conditions representative of those encountered in service. The information, obtained under this program, will be of a form which can be utilized in life prediction methodologies which are based on the concept of damage tolerance as a design philosophy. The experimental investigations and the support of analytical modeling address materials and environments typical of those encountered in service and concentrate on those areas where current life prediction schemes are weakest or totally lacking. The emphasis will be on providing experimental data and modeling the fundamental aspects of fatigue in engine alloys. Innovative ideas are used in the investigations and resolution of existing and anticipated material behavior problems in aircraft turbine engines.

The research effort is subdivided into five interrelated research tasks:

- Experimental Procedures and Test Developments
- Experimental Crack Growth Characteristics
- Mechanical Analysis and Parameter Evaluation
- Model Development and Data Analysis
- Basic Mechanical Properties

These tasks form an umbrella that covers many investigations which support major advances in the development of models for life predictions of engine related cracking problems. The following sections discuss work in progress and work completed in these tasks.

## SECTION 2

### EXPERIMENTAL DEVELOPMENTS

#### 2.1 MEASUREMENT TECHNIQUES

A number of measurement techniques related to material testing were developed or improved during the first year of the contract. Most of these techniques are directed toward crack length determination under various environmental conditions. The techniques are strongly influenced by the accuracy and resolution requirements for the data.

##### 2.1.1 Linear Array Laser Interferometer (LALI)

An enhanced laser interferometer for small scale displacement measurements has been developed. The system is based on an interferometric displacement measurement system developed by Sharpe [1]<sup>+</sup> (see Section 2.2.3). Sharpe subsequently used rotating mirrors to obtain displacement resolution on the order of 10 nm.

The new system replaces the rotating mirrors with solid state linear array image detectors and improved data acquisition speed is obtained through the use of a 32 bit microcomputer and dual channel high speed analog-to-digital converters. The linear array system has approximately the same resolution as the rotating mirror system. The maximum displacement range is limited as a result of the data storage capacity to approximately 40 microns.

##### 2.1.2 Back-Face Strain Compliance for SE(T) Specimen

Nonvisual crack length determination for use in crack growth behavior studies can be accomplished with strain measurements on a single edge notched tension, SE(T), specimen. This method of crack length determination is also well suited for use with closed-loop computer controlled test systems.

---

<sup>+</sup>Numbers in Brackets Refer to References

A finite element analysis was used to determine the theoretical back-face strain values for various crack length to width ratios from 0.2 to 0.8 and a mathematical relationship of crack length ratios versus back-face strain compliance was developed.

In several preliminary tests, the crack lengths for ratios from 0.2 to 0.4 which were calculated from strain compliance were compared to the optically measured values. The compliance crack lengths agreed with the optically measured lengths to within  $\pm 0.002$  in. Additional tests will be conducted for a comparison at larger crack length ratios.

#### 2.1.3 DC Potential on MTS #8 - TMF Testing

A fully automated DC electric potential system for determining crack length under thermal/mechanical test conditions has been developed. H. H. Johnson's [2] formula is used to determine crack length from electric potential for the center crack geometry. The single constant in the formula is determined by entering a known crack length from an alternate measurement method (typically optical) and forcing the formula to yield the measured electric potential. The method has been found to provide excellent crack length data under nonisothermal conditions. Crack length measurements exhibit a scatter band of approximately 0.051 mm compared with 0.127 mm typical for optical measurements at elevated temperatures. Comparison of potential and optical crack lengths shows less than 0.254 mm difference over the entire test. Most of the difference is attributed to crack tip tunneling which is not accounted for optically. To achieve good crack length resolution and low data scatter, precautions were taken to eliminate or minimize the errors in the potential measurement due to thermal effects.

#### 2.1.4 DC Potential for Creep Crack Length Determination

A DC electric potential system was assembled so that crack lengths could be determined in specimens tested at elevated temperatures under constant load. The voltmeter in the

system is accessed by a Tektronix 4051 microcomputer so that data can be acquired automatically. Several preliminary tests have been conducted on CCT specimens of alloy IN718 at 1200°F to evaluate the capabilities of the system. The results appear to be encouraging. Further tests will be conducted to evaluate the accuracy of theoretical calibration relationships between crack lengths and electric potential for CCT and CT specimens.

#### 2.1.5 Specimen Illumination for Crack Length Measurement at 2000°F+

A system was evaluated to determine the possibility of improving the visibility of cracks at temperatures of 2000°F and above. The system consisted of a short wavelength monochromatic light source and a selective optical filter chosen to match the wavelength of the source. In this case, an argon laser and fiber optic probe were used as a movable light source and a metallic coated optical filter with bandpass at 488 nm was used on the viewing microscope to eliminate all light at wavelengths other than the laser light. The short wavelength green argon laser was used because the standard HeNe laser light at 632 nm is close to the wavelength radiated by the hot specimen.

The system was verified on a creep frame at 2000°F using a cracked CCT sample. Results from the laser were compared with results from standard equipment to determine the laser's effectiveness. Using the standard equipment, the crack was nearly invisible; while under the filtered laser light, the crack tip could be seen easily. The laser system worked well under various loading conditions and appears to be a good way to view samples optically at temperatures above 1800°F or where standard techniques are inadequate. In the future, a simple monochromatic light source could be substituted for the laser, thus, reducing the system cost substantially.

### 2.1.6 Elevated Temperature 2000°F+ Furnace

With the requirement to test material at higher temperatures, two prototype furnaces were constructed to achieve an operating temperature of 2000-2200°F. For simplicity, it was determined to make modifications to a previous furnace design which has provided operational temperatures as high as 1600°F. The first prototype was constructed with a used shell from one of the earlier furnaces, which required no additional mechanical attachments for immediate use. The chief modification was to substitute 2200°F heating elements for the older 1800°F elements. Highly efficient ceramic wool insulation was used in the earlier design, so this was retained. Upon operation, it was noted that the outer skin temperature was approximately 500°F. To maintain 2000°F, the furnace operated on a 90% duty cycle.

The second prototype was constructed with a new shell of slightly larger dimensions than the previous design and used the maximum fixture space available in the test frame. A new insulation material which was proported to have much improved insulating properties was used in conjunction with the ceramic wool. Upon operation, the outer skin temperature was approximately 400°F, only a small improvement over the previous model. To maintain 2000°F, this furnace operated on an 80% duty cycle.

Wrapping the exterior with approximately 1.5 inches of fiberglass blanket reduced the heat loss significantly and one could easily touch the outer surface safely. While the extra blanket is cumbersome and not completely satisfactory, 2000-2200°F test temperatures can be achieved.

## 2.2 TEST SYSTEM AUTOMATION

A number of test systems within the laboratory have been automated and some of the existing automation systems have been improved. The efforts in this area are part of a

continuing effort on the part of the University of Dayton Research Institute (UDRI) to maintain the AFWAL/MLLN laboratory at a state-of-the-art level.

#### 2.2.1 Improvements in the C20 System

The usable stroke capacity of the C20 was increased in order to accommodate the testing of high elongation specimens. A vacuum pump has been connected to the air chamber which allows the shaker head to be positioned above center prior to the test.

The vacuum source also makes possible some compressive loading (approximately 1 kip) on the C20. However, only manual control is available for the vacuum at this time.

#### 2.2.2 Installation of VIC-20 on Instron M/M

A VIC-20 microcomputer was installed as a temporary test monitor device on the Instron Major/Minor test frame until an IBM System 9000 unit is delivered. A standard S/N test matrix is currently being run on alloy N4+ at various temperatures and load ratios. The VIC-20 monitors major load, minor load, high temperature, and low temperature interlocks, and interrupts the test in case of failure in any of these systems. The unit has been an economical, simple solution to the temporary lack of more sophisticated computer hardware for the system.

#### 2.2.3 Development of IDG Short Crack Testing System

The determination of short crack mouth opening displacement (CMOD) can be accomplished by using a unique laser interferometric displacement gage (IDG), originally developed by Sharpe et al. [1]. The method utilizes the coherent light of a HeNe laser to make precise measurements of CMOD by monitoring the movement of interference fringes that are formed

by laser light impinging on two pyramid indents that are across the crack as shown in Figure 1. Movement of the indents is related to the movement of fringes that are formed in space. Counting the fringes that pass a fixed observation point produces relative displacement information for the indents.

Resolution of the system has been increased 100 times by monitoring the fractional movement of the fringes in space. This is accomplished by a system that is shown in Figure 2. The system employs servo-controlled rotating mirrors to sweep the fringe patterns across the stationary detectors. This allows the system to monitor the fringe pattern as a function of time.

A software/hardware system was developed to determine the real-time numerical fringe position using a PDP 11/24 minicomputer. The system is able to produce real-time load versus displacement curves with a resolution of 9 nm. A typical load displacement and differential displacement plot from the system is shown in Figure 3. This system has been used in studies of short crack growth, including surface cracks with lengths on the order of 40  $\mu\text{m}$ . The system will also be used to study the threshold condition as a function of the short crack lengths starting from the cracks with lengths on the order of the grain size. A block diagram of the system and a description of the subroutines is given in Appendix A.

In addition to the IDG control software, a routine was developed to replace the short crack growth control program on the IBM PC. The routine performs the following tasks:

- Runs the MTS machine using a programmable function generator.
- Triggers the camera system for automatic surface photographs.
- Stops at selected load for optical viewing.

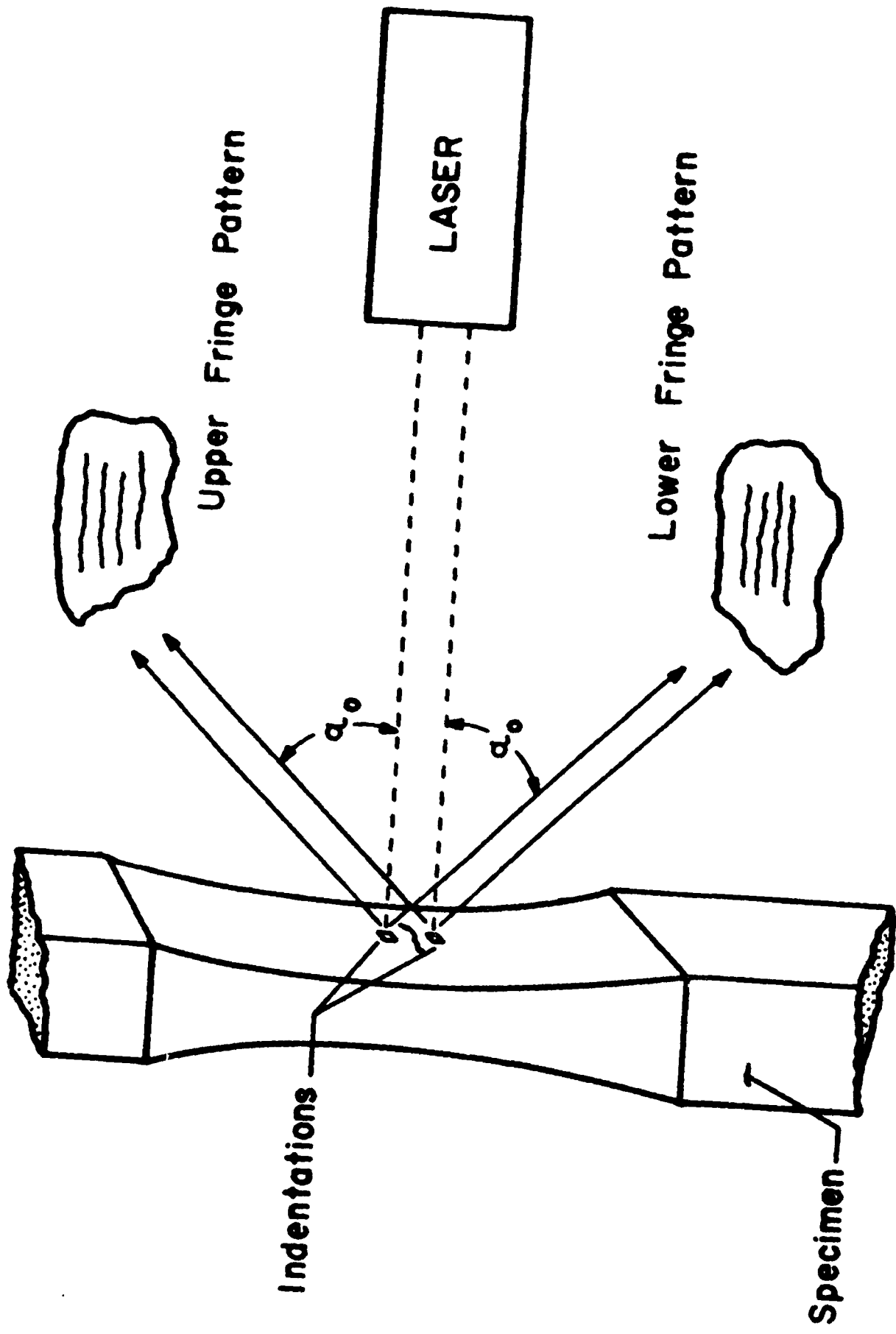


Figure 1. Schematic Illustration of the Principle of Operation of the Interferometric Displacement Gage.

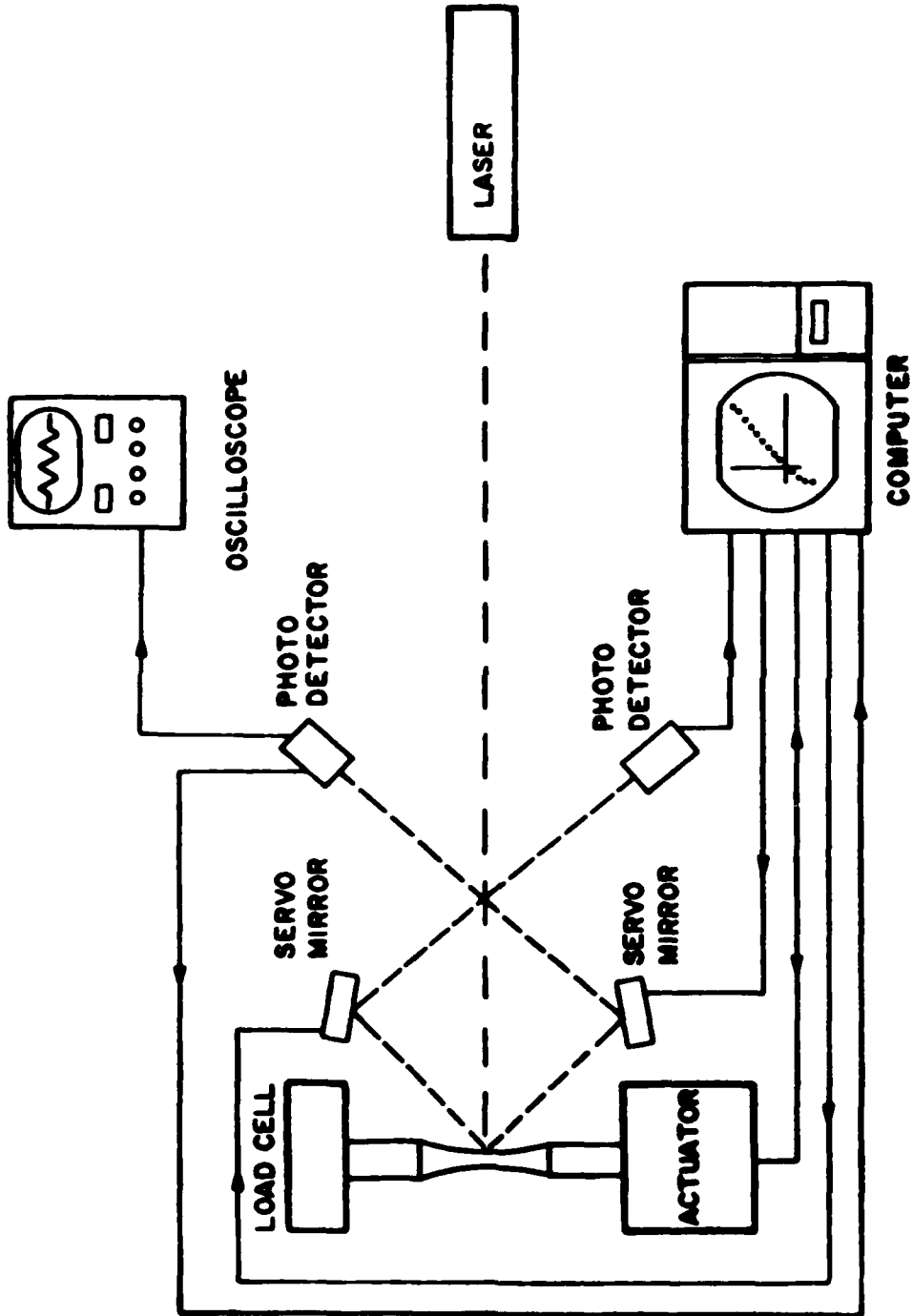


Figure 2. Schematic Illustration of the Computerized Interferometric System.

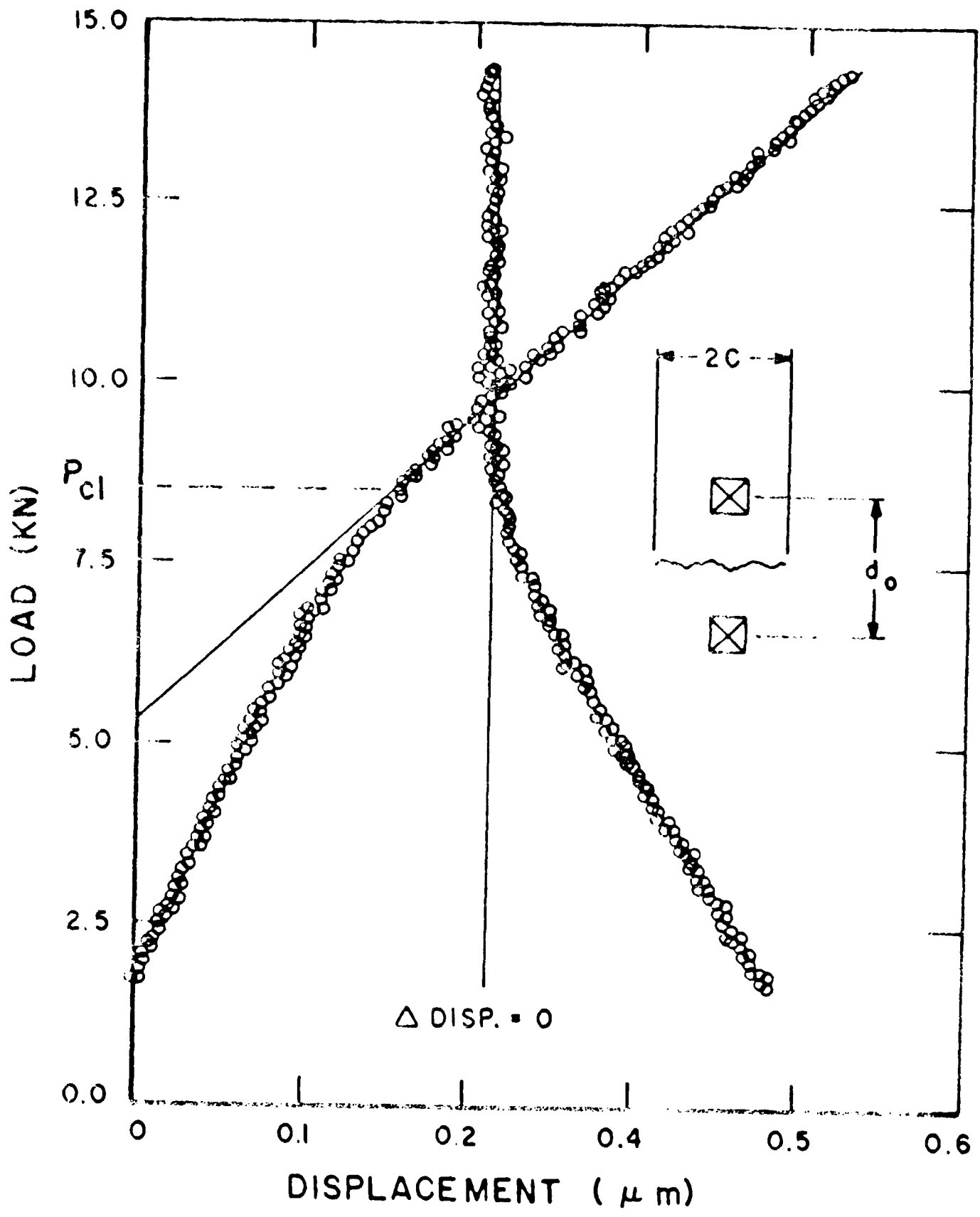


Figure 3. Typical Load Vs Crack-Mouth-Opening-Displacement Data and Differential Data are Shown for a Small Surface Crack Where  $2C \approx 50 \mu\text{m}$  and  $d_0 \approx 50 \mu\text{m}$ .

- Stops at a selected load to allow focusing of the camera/microscope system.
- Communicates with and synchronizes the IDG software with test control functions.

#### 2.2.4 IBM System 9000 Installation on MTS #4 Vacuum System

To provide test control and data acquisition capabilities, an IBM System 9000 microcomputer has been installed on the MTS #4 test frame having a vacuum chamber. The system operates with the same test control software as the other IBM 9000 based systems in the laboratory. However, certain system failures would be catastrophic to the vacuum pump and chamber heating elements should they remain undetected and uncorrected. Additional interlocks will, therefore, be added to the hardware and logic incorporated in the software to protect the vacuum system in case of mechanical failure.

#### 2.2.5 Automated Closure Load Determination

In the past, closure load determination has been a matter of manually examining a load versus displacement plot and estimating the point at which the displacement deviates from the linear data. A new method has been developed in conjunction with the automated test software currently in use on the IBM PC and System 9000 microcomputers in the laboratory. The additional software uses the hysteresis loop and compliance least square fit data. The closure load is determined by determining the load at which the displacement data has deviated from the least square fit by an amount greater than the error band selected by the operator. The algorithm works correctly for displacement errors either positive or negative from the least square fit. By adjusting the displacement error limits, the operator can set up the program to produce reliable closure load data for a number of types of tests. Calculated closure loads are indicated on load versus displacement plots for verification purposes.

The operator must take care to ensure that inappropriate closure load data are not accepted as accurate. Extensometer movement and pin friction may contribute to anomalies in the hysteresis loop. In these cases, the calculated closure loads may not be appropriate.

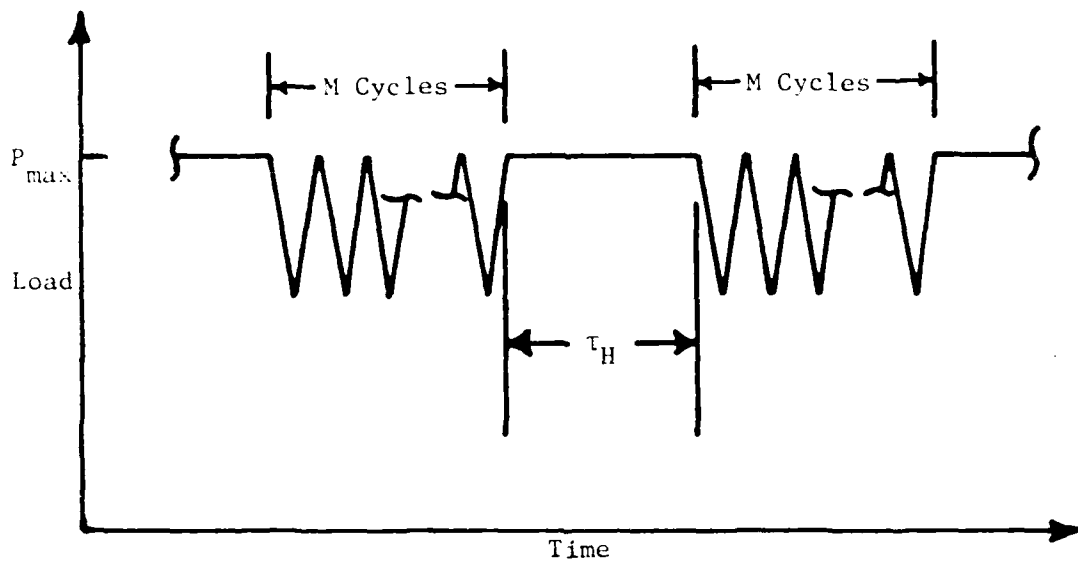
#### 2.2.6 Software Enhancements

Several new control programs and modifications to operational programs were accomplished this past year. For the TEK 4052, software was developed to impose a combination of cyclic and hold-time loads on CT specimens. The loading profiles generated by the software are illustrated in Figure 4.

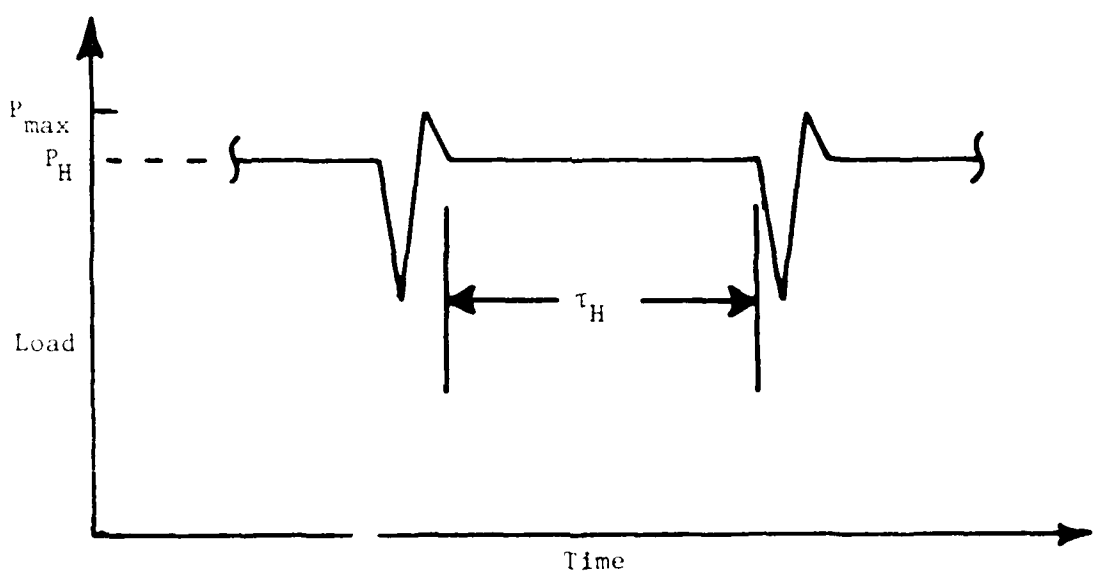
In Figure 4a, a number of cycles ( $M$ ), which is selected by the operator, can be applied to the specimen. Then, a hold-time or dwell period ( $\tau_H$ ), which can be selected by the operator, is applied at the maximum load level. In Figure 4b, a single cyclic load is applied periodically within a sustained load. The time ( $\tau_H$ ) between the loading cycle is adjustable and the load magnitude ( $P_H$ ) during the hold-time can be selected by the operator. The extreme loading conditions for the single cycle load are equal to the hold-time to occur at maximum and minimum load. The loading, shown in Figure 4b, has been used in the investigation described in Section 3.1.7.

A modified TF-34 spectrum load generation has also been incorporated in the control software used on the TEK 4052. This spectrum, shown in Figure 5a, and the Figure 4 loading profiles were used to develop a life prediction model [3].

A simple overload spectrum condition, shown in Figure 5b, was developed for automated control systems using the IBM PC computers. The number of constant amplitude cycles ( $M$ ), the load ratio ( $R$ ), and the overload ratio ( $R_{OL}$ ) can be selected by the operator.

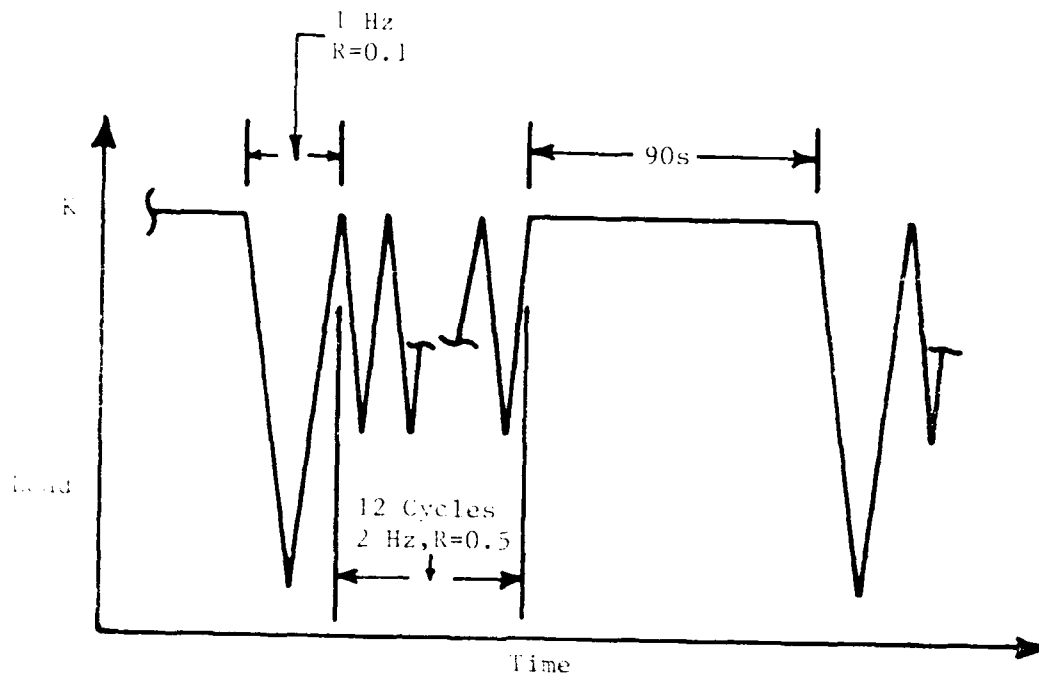


(a)

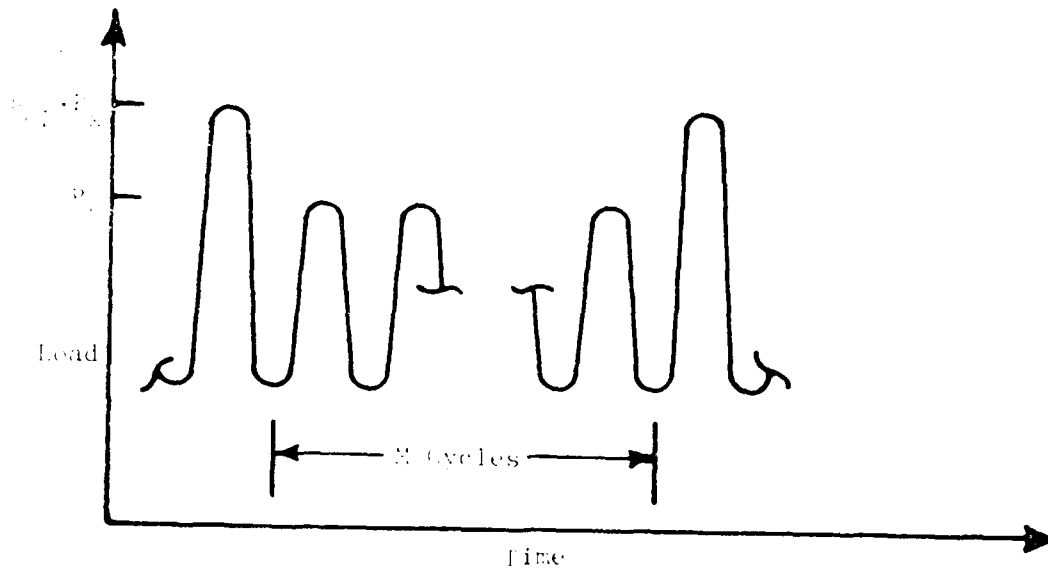


(b)

Figure 4. Combined Cyclic and Hold-Time Loadings Applied by Automated Control Software.



(a)



(b)

Figure 5. (a) Modified TF-34 Spectrum, and (b) Simple Overload Spectrum.

## SECTION 3

### MATERIAL CHARACTERIZATION TESTS

A variety of basic elevated temperature experiments were conducted to improve the characterization and understanding of material response in service conditions. Attempts were made to correlate the mechanical behavior with the original micro-structural characteristic of the material tested. The data were generated on fatigue crack, creep crack growth, and creep rupture as well as hot corrosion behavior of several nickel-base superalloys and titanium alloys.

#### 3.1 FATIGUE CRACK GROWTH TESTING

##### 3.1.1 TMF Baseline Testing

Thermal/mechanical fatigue (TMF) tests have been performed to check out the new TMF test system and to provide baseline data for more advanced TMF test programs. Testing performed to date includes high frequency mechanical loading (600 cpm) combined with a slower thermal cycle (2 cpm). The results of these tests are being analyzed to determine if linear summation models based on isothermal fatigue data can predict crack growth behavior under nonisothermal conditions. Preliminary study indicates that a more complex model incorporating both cycle- and time-dependent behavior may be required to obtain the desired results.

##### 3.1.2 HCF/LCF Initiation in IN718 - C10

Under low cycle fatigue (LCF) loading, a major portion of life is used to initiate a detectable crack. In many components in a modern gas turbine engine, high frequency cyclic loads (HCF) are also present. The influence of HCF loads on the LCF behavior is being investigated in this effort.

A matrix of tests were conducted using axial load fatigue specimens of Inconel 718 sheet at 649°C and 538°C on the C10 electropneumatic shaker. All tests were conducted under load control using an LCF trapezoidal waveshape at 0.33 Hz and  $R = 0.1$  with a 180 s hold-time at maximum load. During the hold-time, a 200 Hz sinusoidal HCF load was superimposed. The amplitude of this minor cycle loading was varied from zero to values where the failure mode was purely high cycle fatigue. Baseline tests were also conducted under LCF loads with no hold-times at the higher temperature and under HCF constant amplitude load at the lower temperature.

The two temperatures were chosen because the material behavior was almost time-dependent at the higher temperature while it was almost entirely cycle-dependent at the lower temperature. Thus, in the absence of the minor cycles, the failure at 649°C was due primarily to sustained load while at 538°C, the hold-times had no effect and failure was due to low cycle fatigue. A limited amount of testing was also planned at an intermediate temperature.

### 3.1.3 HCF/LCF Initiation in N4+ - Instron M/M

Crack initiation tests on single crystal alloy N4+ have been conducted at elevated temperatures on the Instron M/M test frame. Smooth tensile bar geometry specimens in both coated and uncoated surface condition have been tested at a frequency of 250 Hz at temperatures of 1600°F and 2000°F.

A number of experimental difficulties with temperature control, test frame controller breakdown, and finally, a shaker malfunction have delayed completion of this test matrix. The addition of an IBM 9000 microcomputer and IRCON two color pyrometer and the replacement of the test controller are expected to improve the control of the test parameters and to increase the reliability of the test system.

#### 3.1.4 HCF/LCF Initiation on Hastalloy X on C20

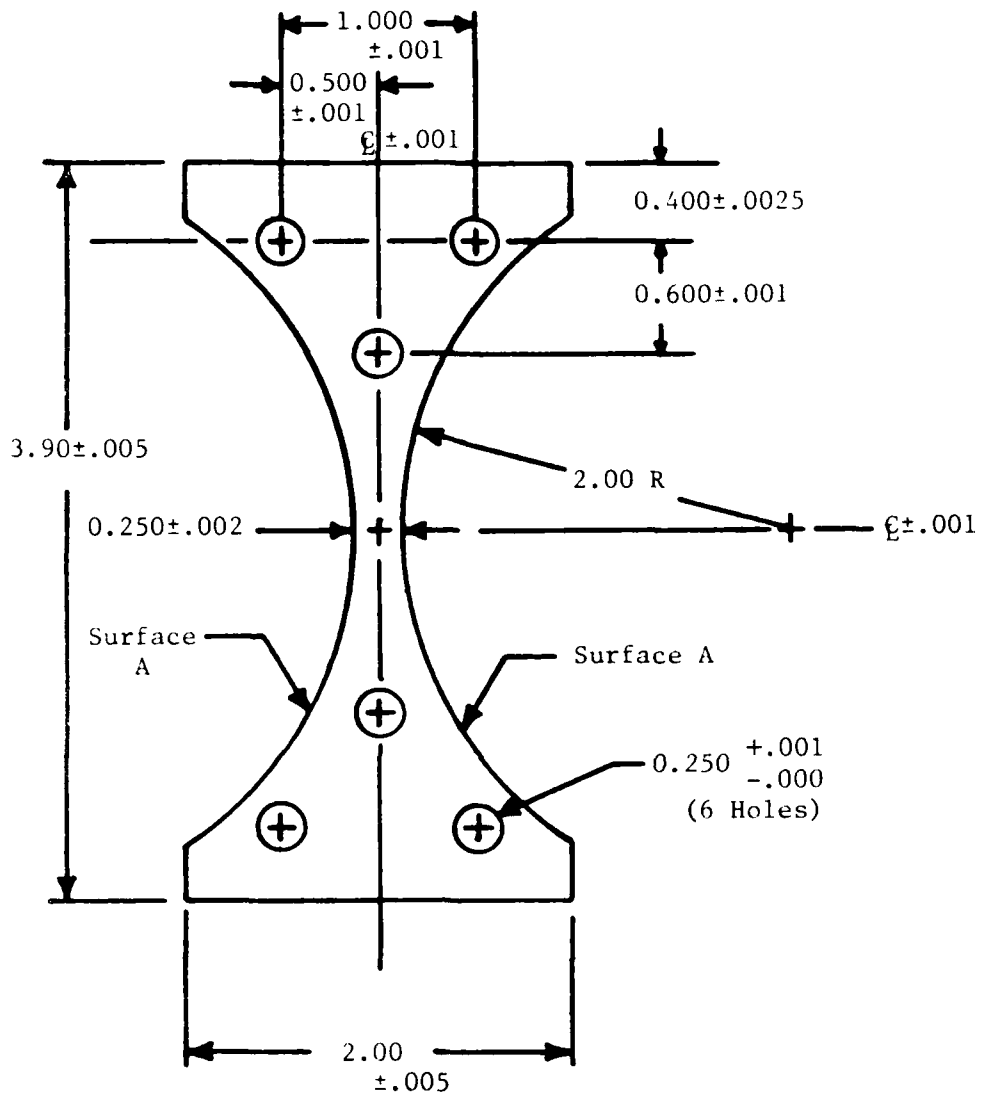
An investigation was initiated to determine the life of Hastalloy X sheet material, 0.5 mm thick, under combined high cycle fatigue and low cycle fatigue (HCF/LCF) load conditions at 800°F. The desired test frequency of HCF loads was in the kiloHertz range. At these frequencies, the loading system and the specimen interact very strongly. Thus, a preliminary task was initiated to evaluate the optimum specimen design and to determine an operating frequency.

The specimen material for the preliminary task was chosen to be steel because it was easy to obtain, the specimens were conveniently fabricated, and the modulus/stiffness was comparable to Hastalloy X at room temperature and at the test temperature. Various sizes of steel specimens, 0.5 mm thick, were tested in the C20 electropneumatic shaker system to evaluate the specimen/system response at frequencies greater than one kiloHertz.

The steel specimens were strain-gaged both for room and 800°F test temperatures to determine the following:

1. Minor load capability as a function of frequency,
2. Percent specimen bending at antinode frequencies, and
3. Calibration factor for force gage at selected test frequencies and load levels.

A frequency of 1120 Hz was chosen, having a slight resonance advantage and low bending. Correlation of strain gage to force gage signals showed a ratio of 1.1:1 which was relatively independent of LCF and HCF load amplitudes. The specimen configuration is shown in Figure 6. Initial testing was plagued with the high elongation of the Hastalloy X which approximately doubled the specimen compliance and resulted in decreased HCF load capability. The beginning HCF load capability for this specimen at 1120 Hz was 18 ksi peak-to-peak



All Dimensions in Inches

Figure 6. HCF/LCF Specimen Configuration.

(± 9 ksi about the mean load) but diminished to 7 ksi peak-to-peak with approximately 30% elongation of the specimen. Testing has been slowed due to electrical and mechanical problems with the system.

#### 3.1.5 Fatigue Crack Growth in Alloy N4

Constant load fatigue crack growth tests were conducted over a temperature range of 538°C, to 871°C (1000°F to 1600°F) for single crystal (SC) Rene' N4 nickel-base superalloy. Crack growth behavior was found to be similar in the Paris law regime for the entire temperature range tested except for a slight increase at 871°C at higher stress intensity range ( $\Delta K$ ) levels. Two distinct modes of fatigue fracture were observed - a flat, featureless, stage II fracture morphology at low  $\Delta K$  levels and a faceted, crystallographic shear, stage I crack mode at higher  $\Delta K$  levels. At 538°C, a transition from stage II to stage I fatigue fracture occurred with increase in  $\Delta K$ , while no such transition was noticed at 649°C and above. The casting defects present in the SC superalloy led to higher crack growth rates at higher temperatures in high  $\Delta K$  regimes. Reference 4 presents further details of this study.

#### 3.1.6 Threshold Evaluation of IN718

Evaluation of crack growth behavior in materials used in gas turbine engines has indicated the existence of both cycle-dependent and time-dependent effects. In determining the life of critical components, both types of effects and their interaction must be taken into consideration in a model. It has been shown that the stress intensity factor is an important parameter in characterizing both the cycle- and the time-dependent behavior in a life prediction model. Since a major portion of life is spent at the low growth rates, the behavior of the material must be well understood in this near-threshold regime. The crack growth behavior can also be time-dependent; thus, the load history and the frequency may affect the near-threshold response.

An experimental program was conducted to evaluate the effects of frequency and hold-time on the near-threshold crack growth behavior of Inconel 718 at 649°C in laboratory air. Frequencies from 0.01 to 30 Hz and hold-times up to 50 s were applied to CT specimens using a computer controlled test machine. Closure loads were determined from digitally acquired load-displacement data. Several tests using high stress ratios ( $R$ ) were used to assess the influence of closure in the low growth rate regime. Various loading histories were employed to achieve near-threshold growth rates.

Several mechanisms known to affect threshold and low crack growth rates were evaluated. Of primary consideration was the influence of closure. Both the oxide formation and the inelastic deformation wake behind the crack tip were evaluated as possible time-dependent mechanisms which can affect the closure behavior. The experimental data generated in this program were used to correlate near-threshold crack growth rates with frequency,  $R$ , and prior load history. Results of this investigation were presented in Reference 5.

### 3.1.7 Effect of Overloads on Alloy IN718

Crack growth rate experiments were conducted on CT specimens of Inconel 718 at 649°C. The loading spectrum consisted of a single 1 Hz cycle at  $R = 0.1$  and a hold-time. The ratio,  $R_{in}$ , of the hold-time load to the maximum load of the fatigue cycle was 1.0, 0.9, 0.8, and 0.5 with hold-times from 0 to 2000 s. Tests were performed under computer controlled constant maximum  $K$  conditions at  $K_{max} = 40$  and 50  $\text{MPa}\sqrt{\text{m}}$ . Data show that for  $R_{in} = 1.0$ , a linear summation model works well, while at  $R_{in} = 0.9$ , there is a measurable retardation effect on the crack growth during the hold-time. For values of  $R_{in}$  less than 0.8, the sustained load crack growth is almost completely retarded. A simple retardation model is proposed which can fit the experimental data and is

based on the concept of an overload plastic zone being produced by the fatigue cycles. It is concluded that hold-times do not contribute to crack growth in this material unless their amplitude is at or near the maximum amplitude of the adjacent fatigue cycles.

#### 3.1.8 Surface Flaw/Short Crack in Ti Alloys

A computerized interferometric displacement gage was used to monitor the crack mouth opening behavior of naturally initiated small fatigue cracks in the high strength alloy Ti-6Al-2Sn-4Zr-6Mo. Complete load versus displacement curves were obtained for naturally initiated semi-circular cracks of surface length as small as 60 microns. For a crack of this size, the maximum crack mouth opening displacement was less than 0.5 microns and the precision of the individual displacement measurements was approximately 0.01 microns. An excellent correlation between crack mouth opening compliance and surface crack length was demonstrated, and the data were shown to agree with an analytical expression for part-through surface cracks. A matrix of experiments was performed for a range of loading conditions, and crack growth data were plotted versus the nominal  $\Delta K$  and effective  $\Delta K$  which was defined using crack closure measurements. Experimental measurements obtained for a small crack indicated that closure often develops discontinuously as the crack initially extends. This behavior was speculated to result from the formation of individual asperities on the fracture surface. In general, the interferometric method proved to be very effective and demonstrated unique capability to monitor the behavior of very small fatigue cracks.

#### 3.1.9 Modeling of IN718 Crack Growth Behavior

A typical engine component service environment consists of combinations of various frequencies, maximum loads,

temperatures, load ratios, and load hold-times. A study of crack growth rate behavior under these conditions leads to methodology and modeling approaches which predict actual service behavior.

A series of tests were performed to acquire a database which could be used to develop and evaluate various crack growth rate models. Data was acquired to determine frequency, temperature, load ratio (R), and maximum stress intensity (K) effects and to correlate these with observed failure of micro-mechanisms. A summary of some of these data is presented in Figure 7. Three distinct regions of crack growth behavior can be identified on the plot:

1. Fully cycle-dependent. The crack grows in a ductile transgranular mode and growth rate is independent of the frequency and mildly dependent on the temperature (T). For this region, the following model is proposed:

$$da/dN = C_c * \text{Exp} (T/T_c) * K^n$$

2. Mixed mode region. The crack grows in both a transgranular and intergranular mode. The crack growth rate is frequency dependent and the following model is proposed for this region:

$$da/dN = C_m * \frac{\text{Exp} (T/T_m)}{f} * K^n$$

3. Fully time-dependent region. The crack growth mode is fully transgranular and is due to oxide embrittlement of the grain boundaries. The crack growth rate is fully frequency dependent (1/f) and the following empirical model is proposed:

$$da/dN = C_t * \frac{\text{Exp} (T/T_t)}{f} * K^n$$

In these models, the C.'s, T.'s, and n are empirical constants.

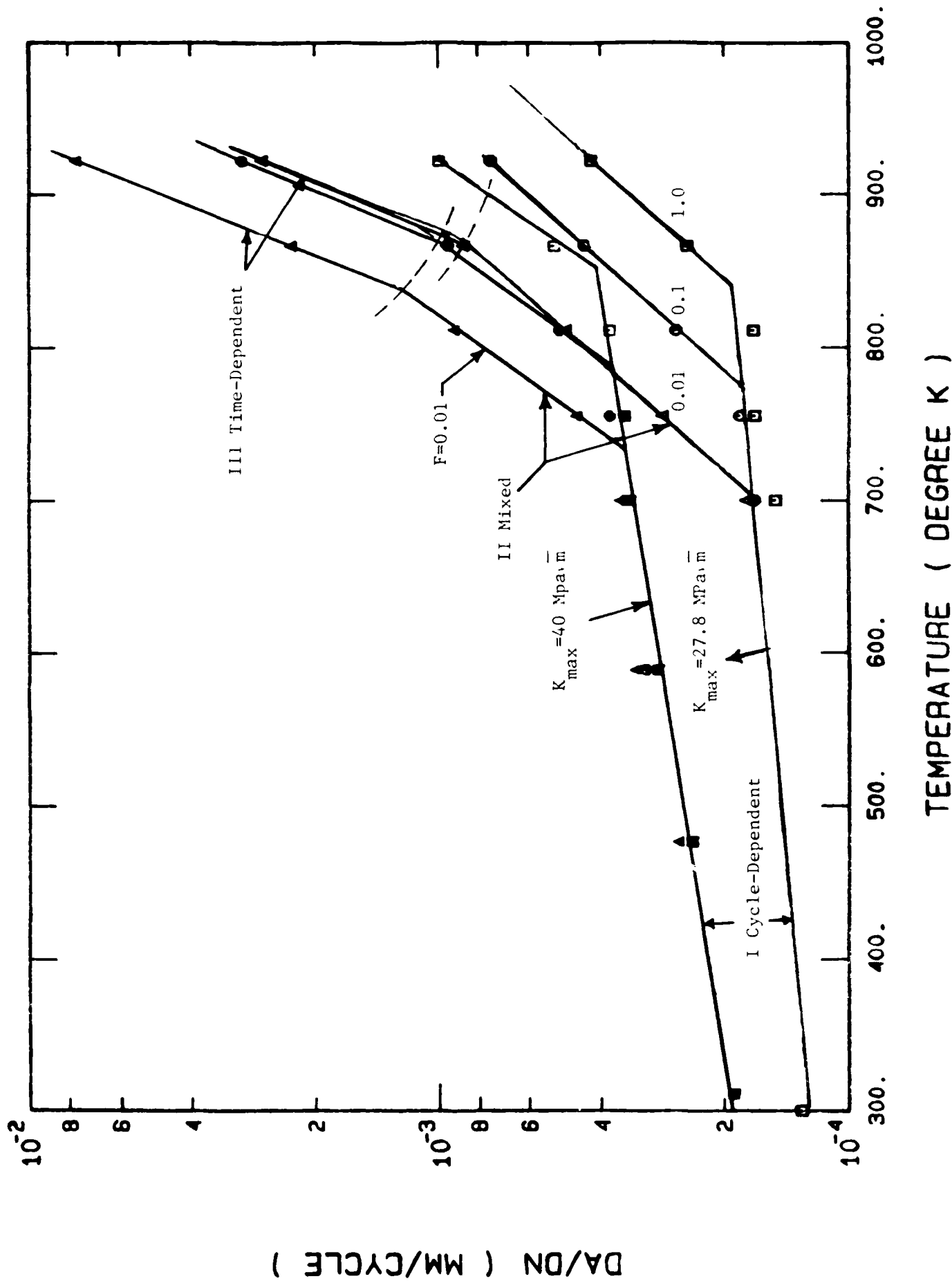


Figure 7. Crack Growth as a Function of Temperature, Frequency, and  $K_{max}$  at  $R=0.1$  for II.718.

Further experiments are being performed at lower frequencies to determine the unknown constants in the proposed models. Threshold crack growth rate data from other laboratory programs will be incorporated into the models where appropriate.

### 3.2 CREEP CRACK GROWTH TESTS

#### 3.2.1 High Temperature Creep Crack Growth in Alloy N4 in Laboratory Air

Creep crack growth (CCG) behavior of advanced nickel-base superalloy Rene' N4 single crystals has been investigated in the temperature range of 1600°F to 1900°F. The objective of this program was to understand the influence of environment as well as the effect of anisotropy on elevated temperature crack growth behavior. Constant load creep crack growth tests were conducted on side-grooved subcompact tension specimens. Crack growth orientations of [100] and [010] with [001] as tensile axis have been tested to investigate the effect of anisotropy. The influence of temperature on the crack growth behavior was studied by analyzing  $K$  versus  $da/dt$  data. The fracture surface was observed under SEM and TEM to identify the creep crack growth mechanism. It appeared that the crack growth was faster when the crack front was oriented perpendicular to the primary dendrites. The details of these results are presented in Reference 6.

#### 3.2.2 High Temperature Creep Crack Growth in Alloy N4 in Vacuum

CCG tests in vacuum were initiated under similar temperature and load conditions utilized for CCG tests in air. The tests started at 1600°F indicated a slower crack growth rate than in laboratory air, hence, the precracking of subsequent specimens was extended from 0.4 inches to nearly 0.44 inches to obtain a higher initial stress intensity value within the load capacity of the pins and grips. There was

premature failure in the first test conducted at 1600°F and 37.5 ksi√in. Crack growth rate and stress intensity information could not be calculated for this test due to insufficient data. Fractographic analysis was conducted on the fracture surface and is discussed in Section 3.2.3.

### 3.2.3 Fracture Surface Analysis of Creep Crack Growth Tested Specimens

The fracture surfaces of the specimens tested in air and vacuum were observed under SEM to determine the failure mechanisms. It appears (although a very small zone of slow creep crack growth was available) that the fracture was transdendritic in vacuum as shown in Figure 8, as compared to interdendritic in laboratory air. Extensive formation of cavities as well as the crystallographic nature of failure is evident in the unstable fracture zone as shown in Figure 9.

## 3.3 CREEP RUPTURE TESTS

### 3.3.1 Creep Rupture Tests of Bare and Coated Alloy N4 in Air

Single crystals of gamma prime precipitation hardened Rene' N4 with tensile axis parallel to [001] were tested under sustained load in the temperature range of 1400°F to 2000°F. The influence of coating was studied by conducting similar tests with bare and coated specimens in laboratory air and tests on bare samples in vacuum. It appears that the coating influences creep rupture life only at higher temperatures by limiting the surface oxidation, since little difference in rupture life was found up to 1600°F where oxidation is negligible. The fracture surfaces of the specimens indicated that the initiation of cracks was more or less random. In some cases, the crack initiated from the internal pores, while surface cracks were also found in other specimens. TEM observations showed a complex substructure of stacking faults within gamma

Crack Growth Direction

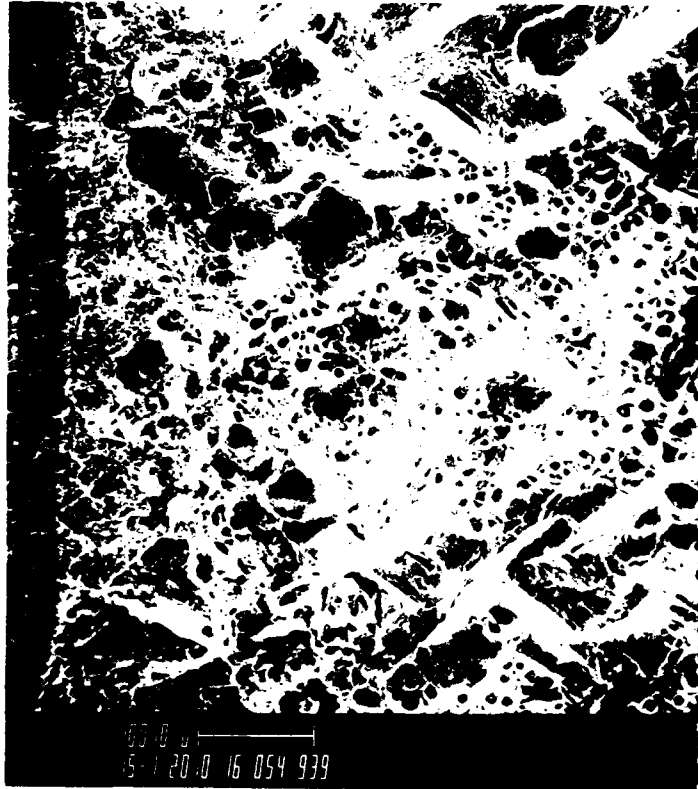


Figure 8. Fracture Surface of Specimen Tested in Vacuum, Showing a Small Zone of Transdendritic Failure.

Crack Growth Direction



Figure 9. Fracture Surface of Specimen Tested in Air, Showing Zone of Interdendritic Failure.

prime precipitate along with dislocation networks on the interface. At higher temperatures above 1800°F, the shearing was mainly by  $a/2$  [110] dislocations. Details of this work are available in Reference 7.

### 3.3.2 Fracture Surface Evaluation of Creep Rupture Specimens

The surface of creep rupture specimens tested at 1600°F and 1800°F under different stresses was observed under optical and SEM microscopes. In some cases, there were indications of the crack initiating from the surface as shown in Figure 10, while in other cases, evidence of multiple initiations from the bulk of the specimen was found. The crack in some cases may have initiated through the shrinkage pores as shown in Figure 11. Transmission electron microscopy analysis was also conducted on specimens ruptured at 1600°F and 1800°F. Thin foils were prepared from slices closest to the fracture surface. The general observation was that the creep substructure at both temperatures had a very high density ( $\rho$ ) of dislocations. Various configurations of stacking faults and extensive regions of network formation are shown in Figure 12. Partial dislocations were also observed. The density of the faults was found to be higher at 1600°F as compared to 1800°F, which is shown in Figure 13 a and b. The two sets of faults formed at 1600°F are more clearly shown in Figure 14. This figure shows a complex arrangement of stacking faults and super dislocations as well as the network of interfacial dislocations. In most cases, the faults were found constricted within the precipitate. However, the formation of microtwins was also evident at 1600°F which is shown in Figure 15. As described earlier, the faults were not found as frequently at 1800°F. The deformation of gamma prime precipitate probably took place by the shear and climb of paired  $a/2$  [110] dislocations at this temperature. Although a complete analysis was not done, individual  $a/2$  [110] dislocations in pairs can be seen in Figure 16.



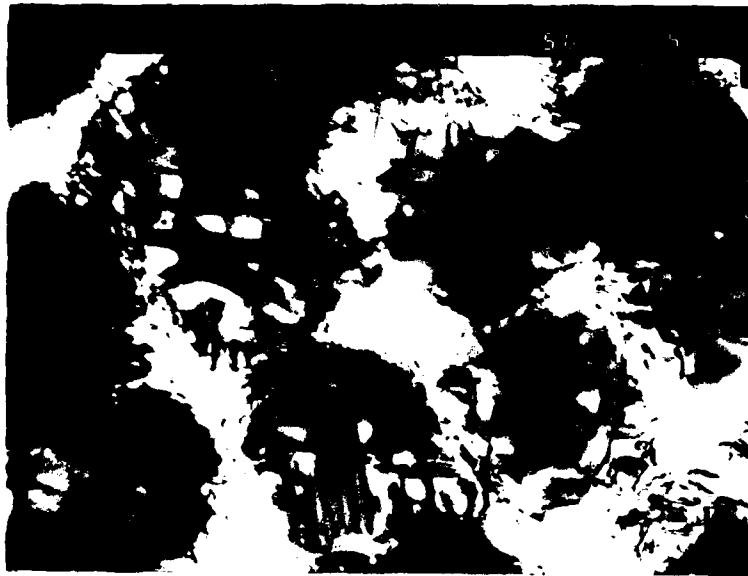
Figure 10. Fracture Surface of a Creep Rupture Specimen Showing Crack Initiation from Surface.



Figure 11. Fracture Surface of a Creep Rupture Specimen Showing Shrinkage Pores.



Figure 12. Complex Faults and Dislocation Networks.



(a)



(b)

Figure 13. (a) Complex Faults at 1800°F and (b) Complex Faults at 1600°F.



Figure 14. Faults and Super-Dislocations.



Figure 15. Microtwins at 1600°F.



Figure 16. Absence of Faults and Evidence of  $a/2$  [110] Dislocation.

### 3.4 HOT CORROSION TESTS

#### 3.4.1 Effect of Hot Corrosion on Creep Rupture Life of IN718

The objective of this study was to examine the effect of stress in the hot corrosion process and the microstructural changes and mechanisms which occur during corrosion-mechanical property interactions. Sustained load creep tests were conducted at a temperature of 1472°F (800°C) in laboratory air at stress levels in the range of 10 ksi to 30 ksi. Smooth, round tensile specimens were coated with a 90% Na<sub>2</sub>/SO<sub>4</sub>/10% NaCl salt mixture by spraying heated specimens with an aqueous salt solution. Tests conducted with salt coated specimens were compared with tests conducted with uncoated specimens. Specimens were subsequently sectioned, and a metallographic analysis of the hot corrosion attack was conducted. Creep data showed a degradation in the creep resistance of IN718 due to the presence of the molten salt environment. The degradation was primarily due to oxide penetration into metal which had been depleted of alloying elements and subsequent cracking along oxide-metal interfaces.

#### 3.4.2 Hot Corrosion in Alloy Rene' 77 and Rene' 80

Static hot corrosion tests on specimens of Rene' 77 and Rene' 80 were conducted. Cylindrical pins were salt coated and tested for 72 hours at a temperature of 1652°F (900°C) in laboratory air. Weight change calculations and measurements of the depth of corrosion attack were made, and a metallographic analysis was done. The test procedure and results are discussed in Reference 8.

## SECTION 4

### ANALYTICAL DEVELOPMENTS

#### 4.1 BACK-FACE STRAIN ON SEN GEOMETRY

A finite element analysis was conducted to determine the theoretical back-face strain (BFS) values for 0.2 to 0.8 crack length to width ratios of a pin loaded SEN specimen. As a result of a previous analysis of a pin loaded SEN specimen, initial meshes had been developed with 104 elements and 356 nodes for the JA code [9]. The meshes incorporated eight (8) triangular elements having quarter point nodes and common vertices at the crack tip to simulate the  $\sqrt{r}$  singularity. Due to symmetry, only half of the SEN specimen was modelled.

The strain calculated on the back-face (opposite the notch) was used to determine a polynomial fit for a relationship between BFS compliance (ratio of strain divided by load)  $C_e$  and crack length ratio. This relationship provides the basis for an automated crack growth control program to determine crack length from BFS compliance.

#### 4.2 ANALYSIS OF DISK-SHAPED COMPACT SPECIMEN

A finite element analysis was conducted on a disk-shaped compact specimen DC(T) to determine crack mouth opening displacement (CMOD) and back-face strain (BFS) for a range of crack lengths. A mesh generation program was developed to generate the input values for crack length to width ratios from 0.25 to 0.8. The finite element code used for the analysis was SNAP [10].

A typical mesh for the DC(T) specimen with  $a/W = 0.5$  is shown in Figure 17. Special triangular elements with quarter point nodes have been used to simulate the  $\sqrt{r}$  singular around the crack tip. The results for the stress intensity factor as a function of crack length compare favorably with values given in the published literature.

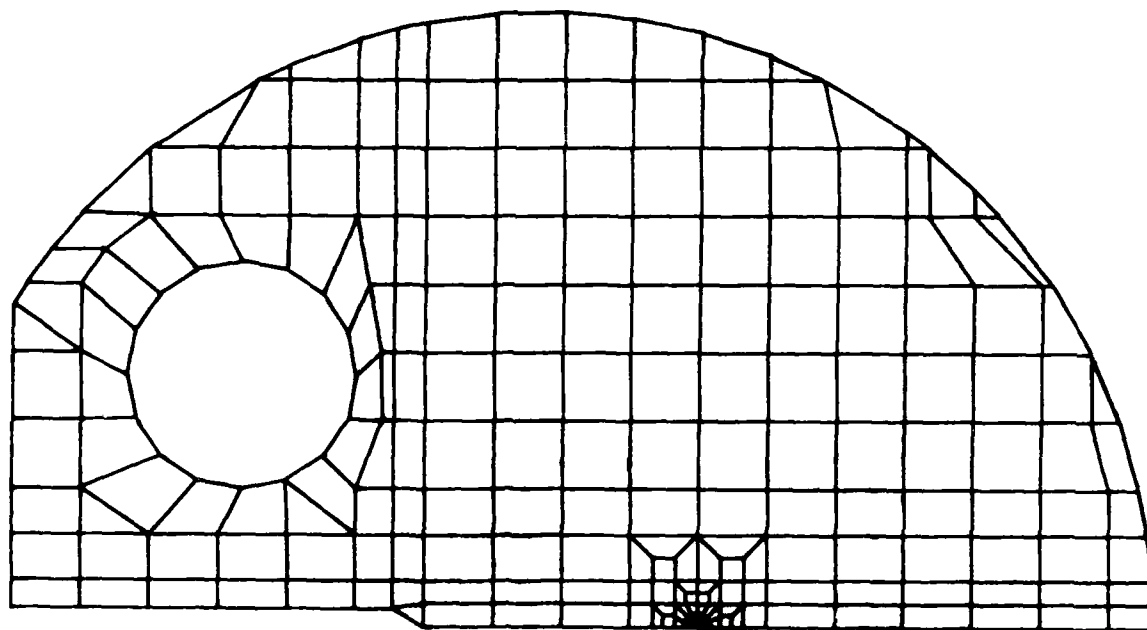


Figure 17. Mesh for Finite Element Analysis of DC(T),  $a/W = 0.5$ , Specimen.

From the finite element results for CMOD and BFS, relationships will be established for the crack length as a function of the CMOD compliance and of the BFS compliance. Then, these relationships can be used in the software for the automated crack growth control of DC(T) specimens.

#### 4.3 THREE DIMENSIONAL ANALYSIS OF CURVED CRACK FRONT

A three dimensional analysis of a curved crack front was initiated using a code based on the alternating finite element technique [11]. Problems in the code developed during the analysis of a nearly straight through-the-thickness crack in a ring specimen. An input file has been generated for a benchmark problem which has been analyzed and reported in the literature. An attempt will be made to operate the code with the benchmark data and the results will be compared to the published values. With this experience, the problems with the input for the original geometry will be investigated.

#### 4.4 VALIDATION OF BODNER-PARTOM ROUTINES IN SNAP

The purpose of this task was to validate a computer algorithm to describe material response using the Bodner-Partom (B-P) constitutive equations [12] in the 'SNAP' finite element program [10]. The validation scheme involved the comparison of cyclic stress-strain response computed by SNAP with the response calculated from the direct solution of B-P equations.

For a trial problem, a tensile strip specimen subjected to cyclic loads was chosen. The corresponding finite element model of the tensile specimen is shown in Figure 18. The specimen was modeled with 6 triangular elements and 8 nodes. A cyclic loading with a peak load of 200 kips at 0.167 Hz and  $R$  (minimum load/maximum load) of -1.0 as shown in Figure 19 was applied to the specimen. The B-P model parameters and equations used in the SNAP simulation are given in Table 1.

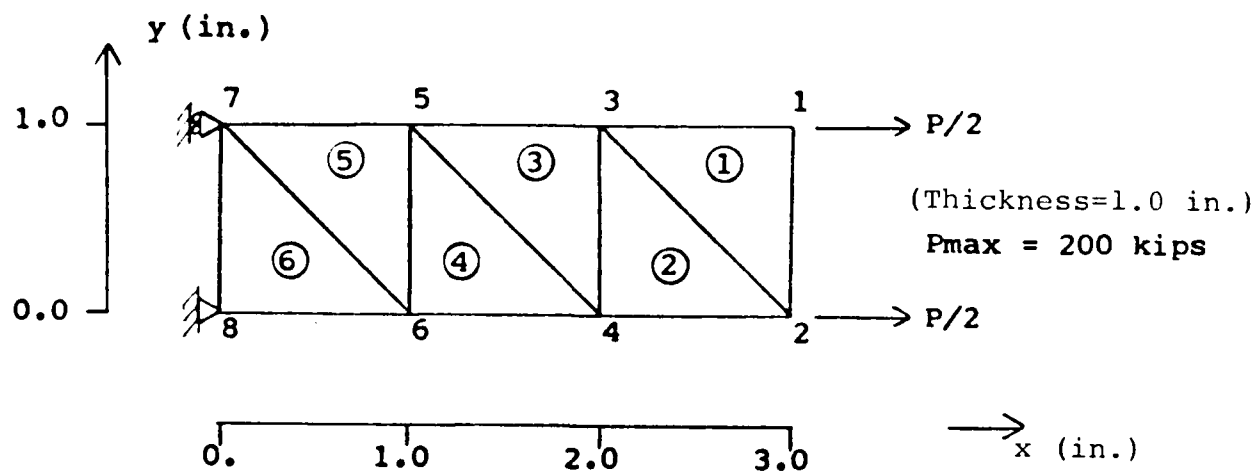


Figure 18. Finite Element Model of a Tensile Strip Specimen.

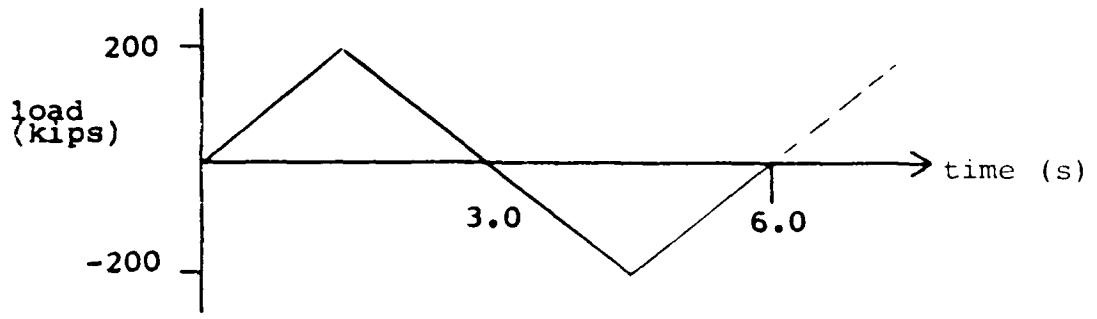


Figure 19. Loading Cycle.

TABLE 1

PARAMETERS FOR THE BODNER-PARTOM  
CONSTITUTIVE EQUATIONS  
(REFERENCE 12)

$$D_0 = 10^4 \text{ s}^{-1}$$

$$n = 0.7$$

$$m = 2.57 \text{ (ksi)}^{-1}$$

$$Z_0 = 915 \text{ ksi, (Initial Value for Z)}$$

$$Z_1 = 1015 \text{ ksi}$$

$$Z_2 = 600 \text{ ksi}$$

$$A = 0.0018 \text{ s}^{-1}$$

$$r = 2.66$$

$$Q = \begin{array}{l} 1, \text{ Fully Isotropic Flow} \\ 0, \text{ Fully Anisotropic Flow} \end{array}$$

Constitutive Equations

$$\dot{\epsilon}^P = \frac{2}{\sqrt{3}} D_0 e^{-\left(\frac{n+1}{2n}\right) (Z/c)^{2n}}$$

$$\dot{Z}^+ = \left[ Q + (1-Q) \frac{\dot{\epsilon}^P}{\dot{\epsilon}^T} \right] \dot{Z} \text{ for tension,}$$

$$\dot{Z}^- = \left[ Q - (1-Q) \frac{\dot{\epsilon}^P}{\dot{\epsilon}^C} \right] \dot{Z} \text{ for compression,}$$

$$\dot{Z} = m(Z_1 - Z) \dot{W}_P - AZ_1 \left( \frac{Z - Z_2}{Z_1} \right)^r,$$

$$\dot{W}_P = \dot{\epsilon}^P$$

Solutions were carried out for five full cycles. For loads below the peak load, the solution converged within two or three iterations. Around the peak load, four to seven iterations were required for convergence. In general, the convergence was reasonably fast during the five cycles of loading. The cyclic stress-strain curve saturated at the second loading cycle as shown in Figure 20. This curve computed by SNAP was directly compared with the results obtained from the direct solution of the B-P equations. The SNAP results compared extremely well with the direct solution (see Figure 20) and the difference was less than one percent. The present results validate the B-P model algorithm in SNAP for its accuracy and numerical efficiency.

#### 4.5 COMPLIANCE EXPRESSIONS FOR CT SPECIMENS

Two empirical equations were developed that express displacement across the crack in a compact type (CT) specimen as a function of crack length and distance behind the crack tip. The coefficients in the equations were generally determined by least square error fit to crack surface displacements obtained from finite element analysis. In one expression, simple types of function which depend on either crack length or distance from the crack tip were combined to form an equation that is similar to a series expansion in two separate variables. The second equation was developed from a combination of the far field behavior of the displacements and a near field fit which incorporates the near tip analytical displacement behavior.

Both equations have application to a broad range of values of crack length and distance from the crack tip. Either equation can be used in conjunction with measurements of displacement across the crack surface to indirectly determine the crack length. More details of this effort are given in Reference 13.

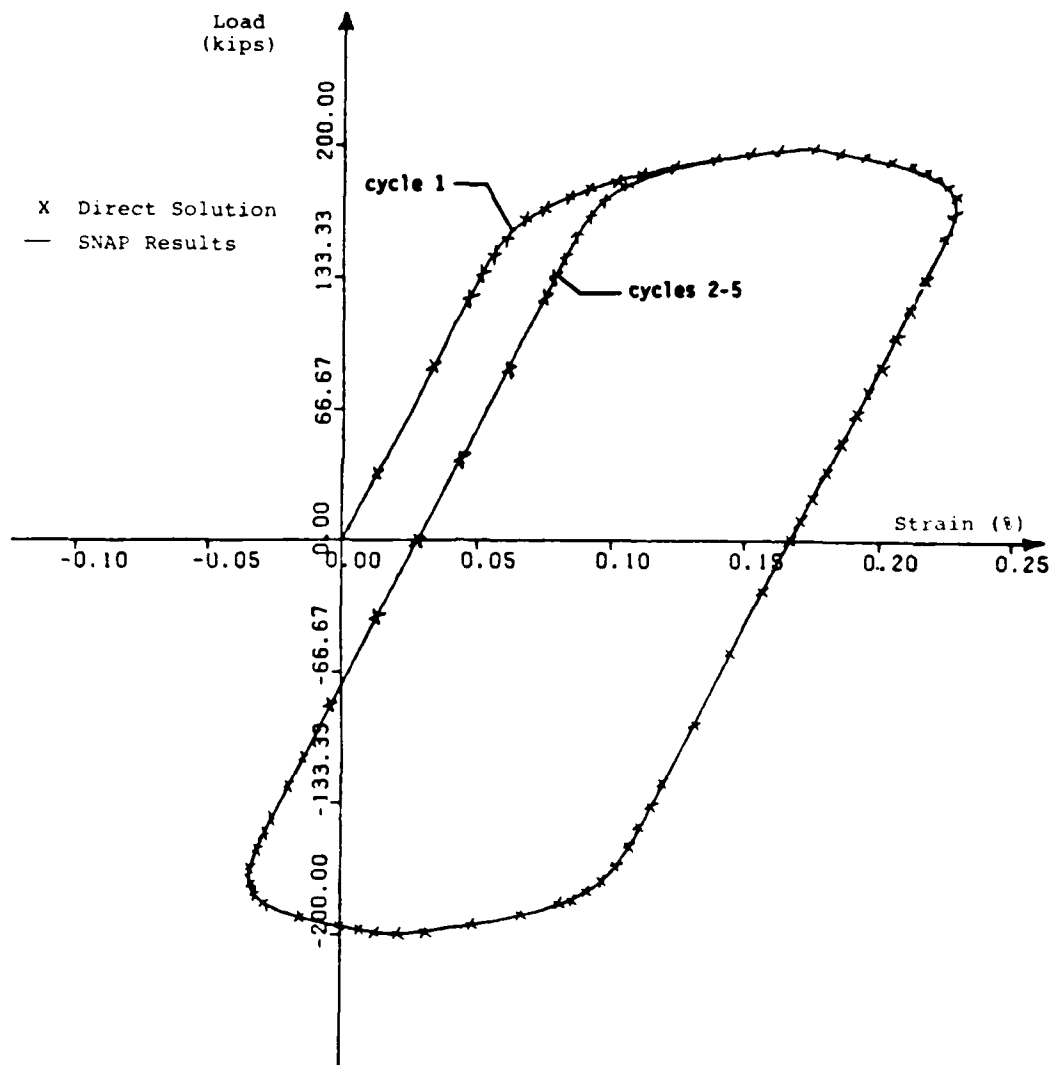


Figure 2C. Comparison Between the SNAP and the Direct Solutions for the Cyclic Loading Response.

## SECTION 5

### DATA MAINTENANCE AND TEST SUPPORT ACTIVITIES

A number of general laboratory support services have been performed as part of the contract. These services make it possible to operate the laboratory in a smooth and efficient manner. In addition, testing support is provided to the MLLS branch as required.

#### 5.1 DATA TRANSMISSION AND STORAGE

The data generated in the laboratory is transmitted to the central laboratory HOST computer for manipulation and storage. The transmission can be made via a number of serial RS232 communication ports attached to various microcomputers at the test stations. A set of data manipulation, reduction, and plotting routines are maintained on the HOST computer for general use. In addition, cartridge tape and removable hard disk media archival facilities are available for all users. All critical data and software, including the system software, are backed up on both tape and disk.

#### 5.2 MLLS BRANCH TEST SUPPORT ACTIVITIES

Tests are conducted in the laboratory to provide basic mechanical property data on existing and developmental materials. The procedures set forth in the ASTM Standard Test Methods are followed for these tests unless otherwise directed by the engineer/scientist. The tests include tensile, elastic modulus, creep and creep rupture, low cycle fatigue, high cycle fatigue, and compression tests.

The types of tests that have been performed during the contractual effort are fatigue crack growth at room temperature, axial fatigue at room temperature, fracture toughness at room

temperature, compression tests at room temperature, creep tests at 565°C, and tensile tests from room temperature to 565°C. These tests were performed on various alloys of aluminum and titanium. After each test, the data were analyzed, documented, and reported to the respective project engineer.

### 5.3 ELECTRONICS FABRICATION AND REPAIR

The nature of the material tests performed within the laboratory periodically requires the development and implementation of electronic equipment and interfaces which are not generally available through commercial vendors. Laboratory electronics personnel are encouraged to maintain a current knowledge of their field to provide new or innovative solutions to electronic measurement or control problems as required. Several electronics packages have been developed in house, including:

- Linear Array Interface Electronics
- Linear Array Power Supplies
- VIC-20 Instron M/M Interlocks
- VIC-20 C20 Interfaces

The primary objective of the contract electronics repair operation is to identify the specific symptoms and if possible, the malfunctioning component. Complicated repair operations are referred to the Base PME section for completion. This arrangement has proved to be efficient for the contract personnel and the PME section.

## REFERENCES

1. Sharpe, W. N., Jr., "Interferometric Surface Strain Measurement," Int. Journal of Nondestructive Testing, Vol. 3, 1971, pp. 59-76.
2. Johnson, H. H., "Calibrating the Electric Potential Method for Studying Slow Crack Growth," Materials Research and Standards, Vol. 5, No. 9, 1965.
3. Weerascoriya, T. and Nicholas, T., "Hold-Time Effects in Elevated Temperature Fatigue Crack Propagation, AFWAL-TR-84-4184, Air Force Wright Aeronautical Laboratories, Wright-Patterson AFB, Ohio, March 1985.
4. Khobaib, M., Venkataraman, S., and Nicholas, T., "Elevated Temperature Fatigue Crack Growth of Rene' N4 Single Crystals," Presented at 18th National Symposium on Fracture Mechanics, Boulder Colorado, 24-27 June 1985.
5. Ashbaugh, N. E., "Time-Dependent and Cycle-Dependent Threshold Evaluation in a Nickel-Base Superalloy," Presented at the 18th National Symposium on Fracture Mechanics, Boulder, Colorado, 24-27 June 1985.
6. Khobaib, M., Venkataraman, S., and Nicholas, T., "An Investigation of Creep Crack Growth of Rene' N4 Advanced Ni-Base Superalloy," Presented at TMS/AIME Fall Meeting, Toronto, Canada, 13-17 October 1985.
7. Khobaib, M. and Nicholas, T., "The Effect of Pack Aluminized Coating on the Creep Behavior of Rene' N4 Single Crystal," to be Presented at TMS/AIME Spring Meeting, March-April 1986.
8. Balsone, S. J., Khobaib, M., and Watt, G. W., "The Effect of Hot Corrosion on Creep Properties of Inconel 718," Presented at TMS/AIME Fall Meeting, Toronto, Canada, October 1985.
9. Ahmad, J., "Two Dimensional Linear Elastic Analysis of Fracture Specimens: User's Manual of a Finite Element Computer Program," AFWAL-TR-80-4008, Air Force Wright Aeronautical Laboratories, Wright-Patterson AFB, Ohio, February 1980.
10. Brockman, R. A., "SNAP: A Simple Nonlinear Analysis Program for Education and Research," UDR-TM-82-06, University of Dayton Research Institute, February 1982.

11. Smith, F. D. and Kullgren, T. E., "Theoretical and Experimental Analysis of Surface Crack Emanating From Fastener Holes," AFFDL-TR-76-104, Air Force Flight Dynamics Laboratory, Wright-Patterson AFB, Ohio, February 1977.
12. Bodner, S. R., "Representation of Time-Dependent Mechanical Behavior of Rene' 95 by Constitutive Equations," AFML-TR-79-4116, Air Force Materials Laboratory, Wright-Patterson AFB, Ohio, August 1979.
13. Enderle, P. R. and Ashbaugh, N. E., "Two Compliance Expressions for Arbitrary Locations Across a Crack in a CT Specimen," AFWAL-TR-85-4074, Air Force Wright Aeronautical Laboratories, Wright-Patterson AFB, Ohio, June 1985.

APPENDIX A  
DESCRIPTION OF IDG SHORT CRACK  
TESTING SYSTEM

## APPENDIX A

### DESCRIPTION OF IDG SHORT CRACK TESTING SYSTEM

The block diagram of the system for controlling the short crack growth test and the rotating mirror interferometric displacement gage is shown in Figure A1. The major components of the system are indicated in the figure.

The main program for operating the rotating mirror IDG initializes the appropriate test parameters and calls the various subroutines. A description of some of the subroutines that were developed for the system is given below.

SCAN - Rotates the mirrors to sweep the fringe pattern across photo detectors and acquires the light intensity data from the detectors.

FNDMIN - Determines the mirror positions for minimum light intensity using a nine point averaging scheme.

CVTAD - Converts the digital voltage values to engineering values.

SND - Calculates the displacement from the fringes positioned at minimum light intensity. This routine also tracks and switches fringes to maintain the center of the fringe pattern on the detectors.

COMP - Calculates the compliance from load versus displacement data and computes the differential displacement data.

PCLCAL - Calculates the closure load automatically based on a statistical procedure.

LDPLOT - Displays the load displacement data curves on a CRT. Closure load, compliance windows, and a line representing the least square compliance fit are also plotted. This routine uses the PLOT10 graphics library.

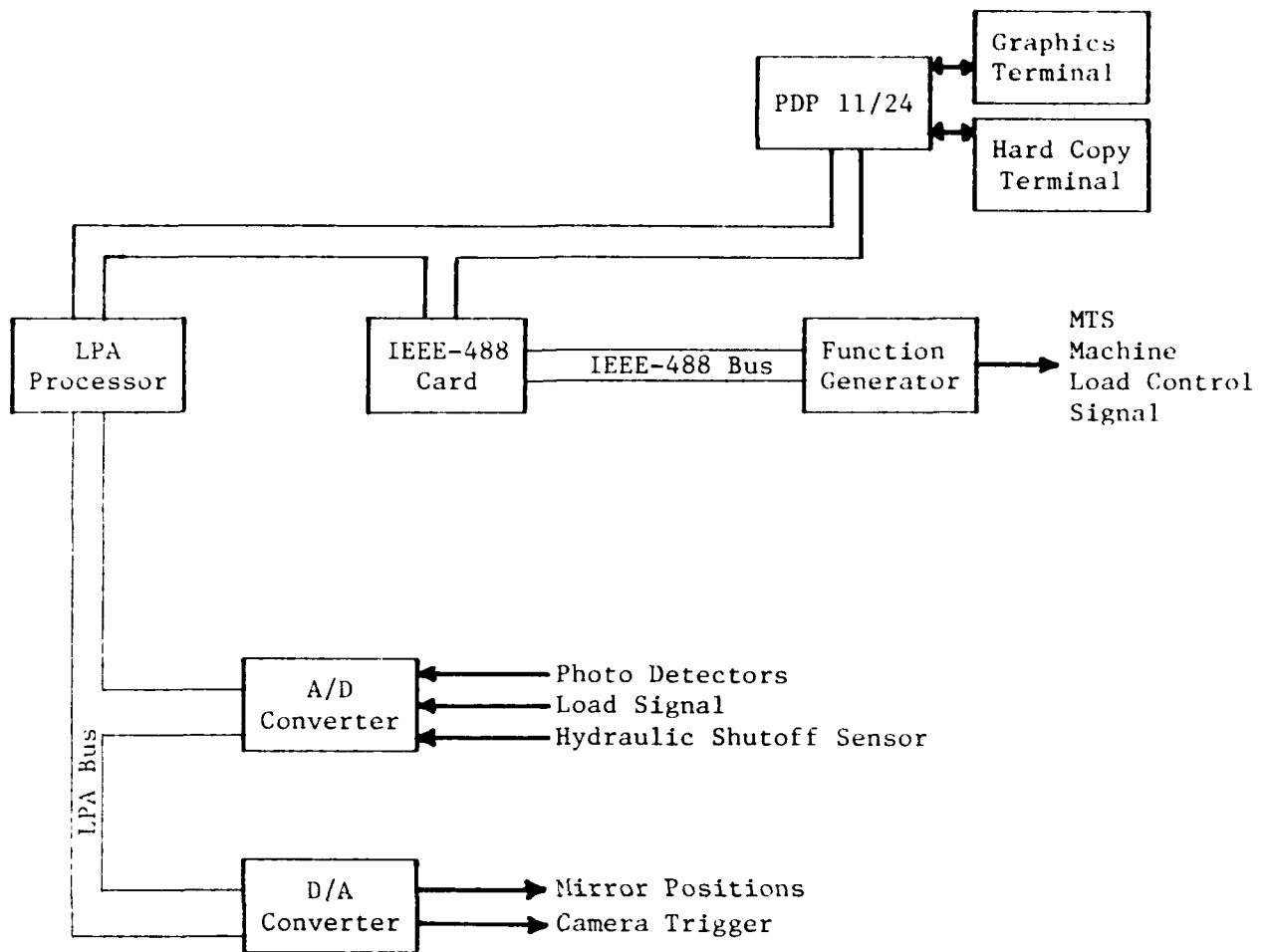


Figure A1. Block Diagram of the Hardware Setup for the MTS/IDG Short Crack System.

LSQREG - Fits a linear least square error line for a given set of data.

CHNGVT - Switches the video terminal between graphics and text mode.

ACALC - Calculates crack length for a surface crack from the given compliance and aspect ratio using an iterative procedure.

ASPCAL - Calculates an aspect ratio for a given compliance and crack length using an iterative procedure.

IDGPLT - Plots given sets of data on the screen.

END

DTIC

8-86